The crystal structure of pectate lyase peli from soft rot pathogen Erwinia chrysanthemi in complex with its substrate

Christophe Crezé, Sandra Castang, Emmanuel Derivery, Richard Haser, Nicole Cotte-Pattat, Vladimir Shevchik, Patrice Gouet

▶ **To cite this version:**

Christophe Crezé, Sandra Castang, Emmanuel Derivery, Richard Haser, Nicole Cotte-Pattat, et al.. The crystal structure of pectate lyase peli from soft rot pathogen Erwinia chrysanthemi in complex with its substrate. Journal of Biological Chemistry, 2008, 283 (26), pp.18260-18268. 10.1074/jbc.M709931200 . hal-00315227

HAL Id: hal-00315227
https://hal.science/hal-00315227v1

Submitted on 15 Oct 2024

HAL is a multi-disciplinary open access archive for the deposit and dissemination of scientific research documents, whether they are published or not. The documents may come from teaching and research institutions in France or abroad, or from public or private research centers.

L'archive ouverte pluridisciplinaire **HAL**, est destinée au dépôt et à la diffusion de documents scientifiques de niveau recherche, publiés ou non, émanant des établissements d'enseignement et de recherche français ou étrangers, des laboratoires publics ou privés.

Distributed under a Creative Commons Attribution 4.0 International License

THE JOURNAL OF BIOLOGICAL CHEMISTRY VOL. 283, NO. 26, pp. 18260–18268, June 27, 2008
© 2008 by The American Society for Biochemistry and Molecular Biology, Inc. Printed in the U.S.A.

The Crystal Structure of Pectate Lyase PelI from Soft Rot Pathogen *Erwinia chrysanthemi* in Complex with Its Substrate*[S]

Received for publication, December 5, 2007, and in revised form, April 21, 2008 Published, JBC Papers in Press, April 22, 2008, DOI 10.1074/jbc.M709931200

Christophe Creze[‡], Sandra Castang[§1], Emmanuel Derivery[‡2], Richard Haser[‡], Nicole Hugouvieux-Cotte-Pattat[§], Vladimir E. Shevchik[§], and Patrice Gouet[‡3]

From the [‡]Laboratoire de BioCristallographie, Institut de Biologie et Chimie des Protéines, CNRS et Université de Lyon, UMR 5086, IFR 128 "BioSciences Gerland-Lyon Sud", F-69367 Lyon Cedex 07 and [§]Unité Microbiologie Adaptation et Pathogénie, UMR 5240 CNRS, Université Lyon 1, F-69622, INSA-Lyon, F-69621 Villeurbanne, France

The crystallographic structure of the family 3 polysaccharide lyase (PL-3) PelI from *Erwinia chrysanthemi* has been solved to 1.45 Å resolution. It consists of an N-terminal domain harboring a fibronectin type III fold linked to a catalytic domain displaying a parallel β-helix topology. The N-terminal domain is located away from the active site and is not involved in the catalytic process. After secretion *in planta*, the two domains are separated by *E. chrysanthemi* proteases. This event turns on the hypersensitive response of the host. The structure of the single catalytic domain determined to 2.1 Å resolution shows that the domain separation unveils a "Velcro"-like motif of asparagines, which might be recognized by a plant receptor. The structure of PelI in complex with its substrate, a tetragalacturonate, has been solved to 2.3 Å resolution. The sugar binds from subsites −2 to +2 in one monomer of the asymmetric unit, although it lies on subsites −1 to +3 in the other. These two "Michaelis complexes" have never been observed simultaneously before and are consistent with the dual mode of bond cleavage in this substrate. The bound sugar adopts a mixed 2_1 and 3_1 helical conformation similar to that reported in inactive mutants from families PL-1 and PL-10. However, our study suggests that the catalytic base in PelI is not a conventional arginine but a lysine as proposed in family PL-9.

Polysaccharide lyases (EC 4.2.2.x) are polysaccharide-degrading enzymes that cleave glycosidic bonds of C_5 uronic acid polymers. They play a central role in the recycling of plant material and are potent virulence factors of plant pathogenic bacteria and fungi. In contrast to the 111 sequence-derived families of glycoside hydrolases, polysaccharide lyases have been grouped into only 18 families in the CAZy data base (1). Five polysaccharide lyase families (PL-1, 2, 3, 9, and 10)[4] contain pectate lyases (EC 4.2.2.2 and EC 4.2.2.9). These enzymes cleave polymeric α-1,4-linked galacturonic acid (GalA) within the pectate component of the cell wall by β-elimination mechanism, leaving an unsaturated C_4–C_5 bond at the newly formed non-reducing end. The activity is maximal in the pH range 8.5–10.5 and is metal ion-dependent; Ca^{2+} is the general cofactor except for the members of the family PL-2, which depend on Co^{2+}, Mn^{2+}, and Ni^{2+} (2, 3). The divalent cation mediates enzyme-substrate interaction by binding between the protein and the sugar (4). Various pectate lyases prefer either polygalacturonic acid or partially methylated pectin as substrate (5, 6).

Atomic structures have been determined for representatives of all polysaccharide lyase families: PL-1 (7–10), PL-2 (3), PL-3 (11), PL-9 (12), and PL-10 (13, 14). They reveal three topologies for the catalytic module: 1) a right-handed parallel β-helix fold common with the families PL-1, PL-3, and PL-9, first observed for family 1 pectate lyase PelC from *Erwinia chrysanthemi* (7); 2) an $(\alpha/\alpha)_7$ toroid in family 2, recently described in pectate lyase YePL2A from *Yersinia enterocolitica* (3); 3) an $(\alpha/\alpha)_3$ toroid in family PL-10, first reported for the catalytic module of the pectate lyase Pel10A from *Cellvibrio japonicus* (14). The superhelix fold is also found in family PL-6 and in the glycoside hydrolase family GH-28, if one considers only enzymes cleaving glycosidic bonds (15–17). The α-barrel folds from families PL-2 and PL-10 are unique among polysaccharide lyases and have limited similarities to a few glycoside hydrolases (18). Interestingly, the structures of inactive mutants from family 1 PelC and family 10 Pel10Acm in complex with oligogalacturonate and Ca^{2+} show a similar pattern of enzyme-substrate interactions in their active sites (4, 14). To a certain extent, this observation could be extended to family 2 YePel2A complexed with trigalacturonate but without a metal cation (3). Such local structural equivalence suggests a common β-elimination mechanism among pectate lyases regardless of the topology of the protein. The catalytic reaction is initiated by an essential basic amino

* This work was supported by grants from the Centre National de la Recherche Scientifique. The costs of publication of this article were defrayed in part by the payment of page charges. This article must therefore be hereby marked "*advertisement*" in accordance with 18 U.S.C. Section 1734 solely to indicate this fact.

The atomic coordinates and structure factors (code 3B4N, 3B90, and 3B8Y) have been deposited in the Protein Data Bank, Research Collaboratory for Structural Bioinformatics, Rutgers University, New Brunswick, NJ (http://www.rcsb.org/).

[S] The on-line version of this article (available at http://www.jbc.org) contains two supplemental tables.

[1] Present address: Division of Infectious Diseases, Children's Hospital, Harvard Medical School, Boston, MA 02115.

[2] Present address: Laboratoire Morphogenèse et Signalisation Cellulaire, UMR144 CNRS/Institut Curie, 26 Rue d'Ulm, 75248 Paris Cedex 05, France.

[3] To whom correspondence should be addressed. Tel.: 33-472722624; Fax: 33-472722616; E-mail: p.gouet@ibcp.fr.

[4] The abbreviations used are: PL, polysaccharide lyase; $GalA_4$, tetragalacturonic acid; Fn, fibronectin; GH, glycoside hydrolase; MES, 4-morpholineethanesulfonic acid; r.m.s.d., root mean square deviation.

This is an open access article under the CC BY license.

acid that abstracts the proton from the carbon C_5. This residue appears to be an arginine in families PL-1 (7–10), PL-2 (3), and PL-10 (13, 14) and a lysine in family PL-9 (12). Whether a lysine or an arginine is the catalytic base for family PL-3 remains to be determined (11).

The enterobacterium *E. chrysanthemi* is a causative agent of soft rot disease in a wide variety of plants. Among a set of pectin-depolymerizing enzymes produced by *Erwinia*, pectate lyases are the major pectinases and play a key role in plant tissue maceration. The pectate lyase PelI belongs to family PL-3 and is the only known example from the *E. chrysanthemi* pectinases that comprises two functional modules, termed the N-terminal domain (residues 20–116) and the catalytic domain (residues 117–344) (6). The close homologue Pel-3 from *Erwinia carotovora* (19) has a similar N-terminal extension, suggesting analogous protein architecture.

PelI possesses a 19-residue signal peptide that is cleaved during export by the Sec system, following which the protein is secreted into the external medium by the type 2 secretion system (20). The two structural modules are separated *in planta* by *E. chrysanthemi* proteases (6). The resulting catalytic domain (residues 117–344) possesses similar enzymatic properties *in vitro* to the full-length protein. However, in contrast to the full-length PelI, it elicits a necrotic reaction associated with an active defense by plants. This hypersensitive response is characteristic of a set of effector proteins secreted by many plant pathogenic bacteria by the type 3 secretion systems (21).

The catalytic domain of PelI shows a sequence identity of 26% with the unique structural representative of the family PL-3, the alkaline pectate lyase Pel-15 of *Bacillus sp.* strain KSM-P15 (11). This protein exhibits the classical superhelical fold, and its putative active site is located in a conserved cleft that stretches along the external core of the superhelix.

Here, we present the crystallographic structures of full-length PelI and that of the single catalytic domain termed $PelI_{cata}$ in order to visualize the rearrangements that likely occur *in planta* after maturation. Furthermore, the associated structure of PelI in complex with a polygalacturonate fragment (a tetragalacturonate $GalA_4$) provides new insight into the catalytical mechanism.

MATERIALS AND METHODS

Protein Purification—PelI was expressed in *Escherichia coli* BL21 (DE3) (Stratagene) cells carrying a high expression plasmid with the *pelI* gene and purified to homogeneity as described before (22). The module $PelI_{cata}$ was obtained by treatment of pure full-length PelI with the *E. chrysanthemi* protease PrtC (6). $PelI_{cata}$ was then separated from the N-terminal domain by chromatography on Protein-Pak CM 8HR (Waters) column equilibrated with 20 mM sodium acetate, 0.1 mM EDTA, pH 5.0 buffer. The protein was eluted with a 0–0.5 M NaCl linear gradient in the same buffer and then concentrated to 15 mg/ml in a Centricon 10 (Amicon) in 10 mM Tris-HCl with 0.1 mM $CaCl_2$.

Construction of Mutant Proteins and Enzyme Assay—Single amino acid mutations were introduced in the PelI sequence by site-directed mutagenesis using the QuikChange kit (Stratagene). The primers used are PelIK224R (5′-ggcggcaaaccggac-a**g**agtgctgcagcacaattcc-3′), PelIK249R (5′-ctgaccggtgaacacggg-a**g**attgtggcgttcctgcgg-3′), PelIR252K (5′-ggtgaacacgggaaattgtg-g**aag**tcctgcggcgactgctcc-3′), and the corresponding reverse complementary primers (mutated bases are in bold). The nucleotide sequences of mutant genes were checked (Genome express). The mutant proteins were produced and extracted from *E. coli* BL21 cells as described above for the wild type PelI. Their amounts were estimated by immunoblotting with PelI antibodies, and then equivalent quantities of each mutant protein and the wild type PelI were used in enzyme assay. Pectate lyase activity was measured spectrophotometrically by monitoring the formation of unsaturated products from pectin. The assay mixture contained 50 mM Tris-HCl, pH 8.5, 1 or 3 mM $CaCl_2$, and 0.5 g·liter^{-1} pectin with a degree of methylation of 45%. The appearance of unsaturated products was monitored at 37 °C over a period of 30 s with 6-s intervals and used to calculate enzyme activity as described (6).

Crystallization—Crystals of PelI were grown as reported previously (22). They belong to space group $P2_1$ with unit-cell parameters $a = 61.6$ Å, $b = 70.7$ Å, $c = 73.4$ Å, $\beta = 112.8°$ and contain two molecules in the asymmetric unit. Crystals of $PelI_{cata}$ were obtained in the same conditions, *i.e.* by the vapor diffusion method from a solution containing 10 mM zinc sulfate, 100 mM MES, pH 6.5, 25% polyethylene glycol 550 (w/v) at a temperature of 292 K. A 1:1 ratio of protein to reservoir solution was used. Crystals belong to space group $P2_12_12_1$ and have cell dimensions $a = 45.4$ Å, $b = 62.6$ Å, $c = 128.1$ Å. The calculated V_m is 1.9 Å^3/Da for two molecules in the asymmetric unit.

The structure of the Michaelis complex was obtained by soaking a crystal of PelI for 24 h in the crystallization buffer depleted in zinc sulfate and with increasing concentrations of $GalA_4$ (1, 2, 3 mM). These successive soakings were performed in calcium-free solutions at pH 6.5 to avoid enzymatic reaction. The soaking experiment induces a significant modification of unit cell parameters up to $a = 61.2$ Å, $b = 68.7$ Å, $c = 73.4$ Å, $\beta = 113.9°$.

X-ray Diffraction Experiments and Structure Determinations—Before data collection, all crystals were rapidly transferred into a cryoprotectant solution consisting of the crystallization solution plus 15% (v/v) ethylene glycol. Synchrotron data were collected at 100 K at European Synchrotron Radiation Facility beamlines, Grenoble, France. The programs XDS and XSCALE were used for data reduction and scaling (statistics in Table 1). 5% of randomly selected reflections were kept apart for cross-validation, and the crystallographic refinement was performed with CNS using the method of slow cooling simulated annealing (23). After each cycle, the model was manually improved using the graphic program *TURBO FRODO* (24). Final statistics are presented in Table 1. The quality of the refined structures was assessed with PROCHECK (25).

PelI—The first model of PelI was obtained at 1.6 Å resolution by single wavelength anomalous dispersion phasing of a gold derivative (22). A native structure was subsequently determined to 1.45 Å resolution from synchrotron data collected at 100 K at a wavelength of 0.94 Å at beamline BM30A. The crystallographic refinement yields an *R*-factor of 16.8% (R_{free} 19.5%). The model contains two monomers, termed A and B. Residues 108–118 were not visible in electron density maps.

TABLE 1

Data collection and refinement statistics

Values in parentheses are for the high resolution shell. ESRF, European Synchrotron Radiation Facility.

	PelI	PelI-GalA4	$PelI_{cata}$
Data collection			
Synchrotron beamline	BM30A, ESRF	ID14–3, ESRF	ID14–3, ESRF
Wavelength (Å)	0.940	0.931	0.931
Space group	$P2_1$	$P2_1$	$P2_12_12_1$
Unit-cell parameters (Å,°)	$a = 61.6$, $b = 70.7$, $c = 73.4$, $\beta = 112.8$	$a = 61.2$, $b = 68.7$, $c = 73.4$ Å, $\beta = 113.9$	$a = 45.4$, $b = 62.6$, $c = 128.1$
Resolution limit	1.45 (1.5-1.45)	2.3 (2.4-2.3)	2.1 (2.5-2.1)
Number of measurements	379,012 (35,039)	91,763 (10,920)	72,076 (7,117)
Unique reflections	102,436 (9,931)	24,759 (2,948)	20,021 (2,172)
Completeness (%)	99.5 (99.8)	99.0 (99.0)	91.9 (77.8)
R_{sym} $(I)^a$ (%)	6.5 (33.0)	5.0 (23.9)	10.8 (18.6)
$I/\sigma(I)$	10.6 (5.4)	18.4 (5.6)	8.0 (5.3)
Crystallographic refinement			
Asymmetric unit content	(2 monomers)	(2 monomers)	(2 monomers)
Number of protein atoms (non-hydrogen)	4,746	4,500	3,330
Number of water molecules	752	171	325
Cations	2 Ca^{2+}, 6 Zn^{2+}	1 Ca^{2+}, 1 Zn^{2+}	2 Ca^{2+}, 4 Zn^{2+}
Other non-hydrogen atoms	33	98	10
Overall *B*-factor (Å^2)	17	37	18
R_{factor}/R_{free} ^{b} (%)	17.5/19.8	19.8/25.3	21.0/27.3
Stereochemical quality of the model			
r.m.s.d. bond lengths (Å)	0.006	0.007	0.006
r.m.s.d. bond angle (°)	1.4	1.3	1.4
Ramachandran plot (allowed)	533 (99.1%)	505 (99.4%)	371 (99.2%)
Ramachandran plot (generously allowed)	5 (0.9%)	3 (0.6%)	3 (0.8%)

[a] $R_{sym} = \sum_h \sum |I_j - \langle I \rangle| / \sum_h \sum I_j$.
[b] R_{factor} and R_{free} are given by $\sum |F_{obs} - F_{calc}| / \sum F_{obs}$.

According to geometric criteria and to the highest peaks in the $2F_o - F_c$ maps, five Zn^{2+} and two Ca^{2+} ions substitute the seven gold ions observed in the derivative structure. Zn^{2+} ions were further identified by collecting synchrotron data around the zinc K edge and calculating anomalous difference Fourier maps. An extra Zn^{2+} ion was positioned in the final structure as well as one SO_4^{2-}, seven ethylene glycol, and 752 water molecules.

$PelI_{cata}$—Data were collected to 2.1 Å resolution at beamline ID14–3. The structure was solved by molecular replacement using the program AMoRe (26) and a two-body search taking as a model the catalytic domain from the structure of PelI (residues 119–344). The first two residues of $PelI_{cata}$ (residues 117–118) are not visible in electron density maps as in the PelI structure. The final *R*-factor is 20.4% (R_{free} 27.1%). Two Ca^{2+} and four Zn^{2+} are observed at positions similar to those of PelI. Two SO_4^{2-} and 325 water molecules have been placed in the asymmetric unit.

PelI-$GalA_4$—Data were collected to 2.3 Å resolution at a wavelength of 0.93 Å at beamline ID14–3. Attempts to solve the structure of the complex by a crystallographic rigid body refinement were unsuccessful due to non-isomorphous crystals (shift in β angle). The structure was solved by molecular replacement using the program AMoRe (26) and a two-body search based on the substrate-free structure. $F_o - F_c$ maps were inspected after crystallographic refinement using CNS. The tetrasaccharide bound to molecule A is unambiguously defined in electron density, whereas the one bound to molecule B is weakly defined at its non-reducing end. The four sugar rings of the two ligands were built and oriented in the electron density. No electron density was found for segments 148–150 and 216–222 from monomer A and segments 77–81, 145–150, and 215–222 from monomer B. These amino acids were deleted from the refined structure as well as one Ca^{2+} and five Zn^{2+} ions. Further cycles of crystallographic refinement yield an *R*-factor of 20.0% (R_{free} 27.9%). The final model contains two $GalA_4$, one Ca^{2+} ion, one Zn^{2+} ion, and 171 water molecules.

Structure Analysis—Secondary structure elements were assigned according to main-chain hydrogen bonds and φ/ψ angles calculated with STRIDE (27). Pair-wise structure comparison was accomplished with DaliLite (28). Images of sequence alignments were prepared using ESPript/ENDscript (29). Interactions between tetragalacturonate and PelI were examined with LIGPLOT (30). Other images were generated with Molscript/Bobscript (31, 32). Atomic coordinates and structure factors of PelI, $PelI_{cata}$, and PelI-$GalA_4$ have been deposited in the Protein Data Bank (PDB) under the codes 3B4N, 3B90, and 3B8Y, respectively.

RESULTS AND DISCUSSION

Overall Fold of PelI—The structure of full-length PelI has been determined to 1.45 Å resolution. The protein crystallizes with two monomers, A and B, in the asymmetric unit but is monomeric in solution according to gel filtration experiments (not shown). The two monomers A and B are very similar, and their C^α traces can be superimposed with a root mean square deviation (r.m.s.d.) of 0.4 Å.

PelI is composed of a fibronectin type III domain (Fn3D) at its N terminus (residues 20–107) fused to a catalytic domain that displays a parallel β-helix fold (residues 119–331). The connecting segment where cleavage by *E. chrysanthemi* proteases occurs (residues 108–118) (6) was not observed in the density and is not modeled. This linker is also predicted as natively disordered by the Regional Order Neural Network server (33), and the crystallographic packing was carefully examined to identify the biological monomer.

The more plausible arrangement of entire protein is presented in Fig. 1*A*. It possesses the largest buried interface between the two domains, 750 Å^2, as well as the shortest dis-

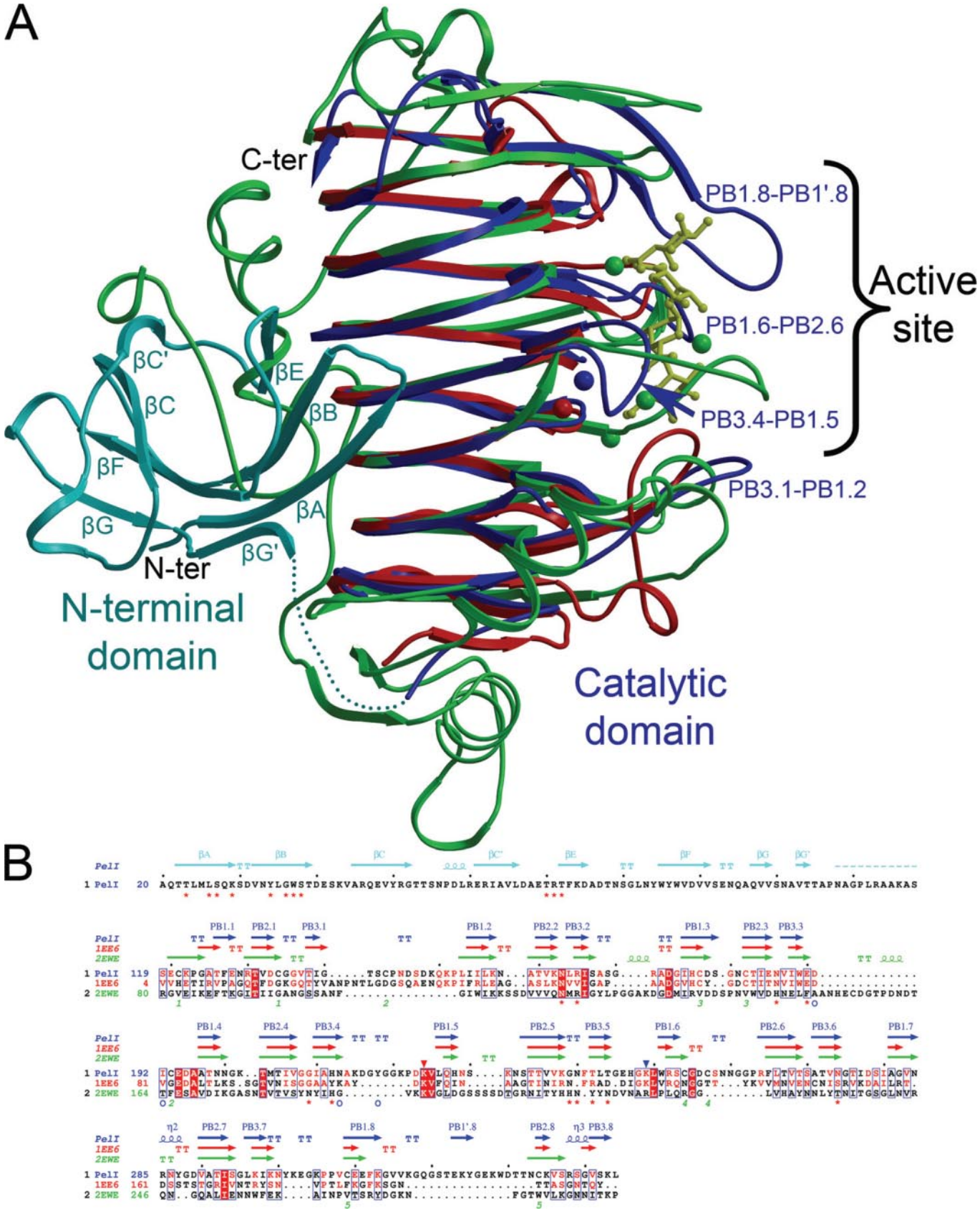

FIGURE 1. **Structural alignment of the catalytic domain of Pell.** *A,* superimposition of the catalytic domain of Pell (*blue*) with Pel15 (*red*) (Protein Data Bank code 1EE6) and PelC (*green*) (Protein Data Bank code 2EWE). Bound calcium ions are shown in Pell, Pel15, and PelC with *blue*, *red*, and *green spheres*, respectively. The bound sugar in PelC is shown in *yellow*. The disordered linker in Pell is shown by a *dashed line*. *B,* structure-based sequence alignment with secondary structure elements. *Top*, *red* and *blue triangles* indicate the putative catalytic residue of Pell and PelC, respectively. *Bottom*, *green numbers*, *red stars*, and *blue circles* indicate Pell disulfide bridges, residues at the interdomain interface (contact distances <3.2 Å), and residues coordinated to a Ca^{2+} ion, respectively.

tance between residues 107 and 119, 23 Å. Such spacing agrees with the 11 missing residues. The occluded face of the catalytic domain is also partially covered in numerous polysaccharide lyases by N-terminal or C-terminal extensions. Moreover, this arrangement between domains evokes the one recently described in a modular bacterial glycoside hydrolase YeGH28 (Protein Data Bank code 2UVE) (16). The Fn3 domain is bound to the opposite of the active site in both proteins but is oriented perpendicularly to the β-helix axis in PelI and parallel in YeGH28.

Fn3 Domain—The N-terminal domain of PelI exhibits a conventional seven-stranded Fn3 fold with a Greek key motif composed of four β-strands termed βC, βC′, βF, and βG (Fig. 1). As reported in some other animal and bacterial Fn3Ds, the last strand βG is split into two short strands (34). The Fn3D does not contain any disulfide bonds and interacts with the catalytic domain via its flat βA, βB, βE, façade (Fig. 1*A*). Two hydrophobic residues, Met^{25} and Tyr^{34}, give extensive contacts at this interface, whereas polar residues mediate hydrogen bonds (Ser^{27}, Ser^{38}, and Thr^{72}, Fig. 1*B*).

A structural search performed with the DALI server shows that this N-terminal domain superimposes with the best match on an Fn3 module of a neural cell adhesion molecule (r.m.s.d. of 2 Å for 85 aligned C^{α} with an amino acid identity of 13%) (Protein Data Bank code 1CFB) (35). It superimposes also extremely well on the Fn3D of the modular YeGH28 polygalacturonase (16), which includes an additional helix-loop-helix motif that further stabilizes the interdomain interface (r.m.s.d. of 2 Å for 79 aligned C^{α} and a sequence identity of 11%).

Fn3Ds are found in many eukaryotic proteins, where they are frequently implicated in cell adhesion and signaling processes (36). They display a variety of binding modes with other proteins, especially via their BC, C′E, and FG loops (37, 38). Fn3Ds have also been reported in bacterial carbohydrate active enzymes, where they may act as spacers between sugar-binding and catalytic domains (34). It has also been suggested that they can help binding of sugar groups or promote hydrolysis (39, 40). However, the distinctive features of carbohydrate binding modules such as a large aromatic platform or a bound Ca^{2+} (41) are not detected on the Fn3D surface of PelI. Moreover, PelI displays the same enzyme activity on pectin regardless of the presence of its N-terminal domain (6). In addition, following crystal-soaking experiments, a pectin fragment, tetragalacturonate $GalA_4$, has been detected only within the catalytic domain, but not in the Fn3D of PelI (see below).

Thus, there is no evidence of direct involvement of this Fn3D (or any other modular carbohydrate active enzymes) in polysaccharide recognition and degradation. On the other hand, eukaryotic Fn3Ds are known for their ability to interact with cell receptors, and this bacterial module may have been a potential pathogen elicitor. However, the hypersensitive response of the plant following the proteolytic cleavage of PelI seems to be triggered by the sole catalytic domain freed from the Fn3D (6).

Catalytic Domain—The catalytic domain is made of eight coils stacked on top of one another (Fig. 1). As in pectate lyases of families 1, 3, and 9, each coil contains three consecutives strand-turn motifs termed $(PBn\text{-}Tn)_{n=1,3}$ (7, 8, 12). The characteristic ladders of inward-facing asparagines observed in family PL-1 and PL-9 within regular stacked turns (7, 12) are absent in PelI as in Pel-15 of the same family PL-3 (11). The stability of the cylindrical core is ensured by inner stacks of aliphatic residues and by five disulfide bonds (highlighted in Fig. 1*B*).

The structures of PelI and Pel-15 superimpose well on each other with a r.m.s.d. of 1.7 Å on 177 C^{α} atoms of 226 (Fig. 1*A*). The main differences lie in the two extremities of the β-helix. The catalytic domain of PelI begins with a portion of random coil whereas Pel-15 harbors a β-strand. This feature might be related to the proximity of the cleavage site in PelI and increases accessibility to proteases. The unique disulfide bond of Pel-15 is conserved in PelI in positions Cys^{177} and Cys^{182}. Finally, PelI displays in its C-terminal a distinctive β-hairpin made of strands PB1.8 and PB1′.8 (Fig. 1). The structure of PelI is more distantly related to that of PelC of family PL-1. 176 C^{α} atoms of 226 overlap with a r.m.s.d. of 2.9 Å, and the sequence identity is only 16%. Two disulfide bonds of PelC maintaining extended loops have no structural equivalents in PelI.

Turns $(Tn)_{n=1,3}$ of the β-superhelix generally start by an amino acid in the conformation of a left-handed α helix (αL). The secondary structure assignment of Fig. 1*B* shows that several turns T of PelI and Pel-15 are made of a single amino acid in αL conformation, which sharply bends the solenoid fold. Of particular interest, the T2 amino acids from coils 2 to 5 line up at the surface of the superhelix (Asn^{163}, Asn^{186}, Gly^{218}, Asn^{240}) and form a highly accessible "Velcro"-like motif of asparagines that anchors the Fn3D. The 2.1 Å structure of the catalytic domain alone, $PelI_{cata}$, has been determined. This structure is quasi-equivalent to that of PelI and demonstrates that this region retains its rigidity when the Fn3D is removed. Hence, this T2 pattern of outward-facing asparagines (NNGN) located in the interdomain interface of full-length PelI becomes accessible after proteolytic maturation. It then might be recognized by an unknown receptor of the infected plant, leading to the defense response.

Ca^{2+} and Zn^{2+} Ions—Calcium ions are essential for the catalytic mechanism of all pectate lyases except the family PL-2, which employs other divalent metal cations (2, 3). They may neutralize the charges of the acidic substrate as observed in the inactive mutant R218K of PelC and pentagalacturonate $GalA_5$ that possesses four Ca^{2+} ions in the binding site (4). PelI was purified in the presence of calcium and was crystallized at pH 6.5 with zinc sulfate (22). One Ca^{2+} ion is present in an equivalent position in each molecule A and B of PelI and $PelI_{cata}$. It binds to an external region of the β-superhelix and coordinates the main-chain carbonyl O of Ile^{192} and Tyr^{218} and the side-chain Oδ of Asp^{191} and Asn^{213}.

In molecule A of PelI, the Ca^{2+} ion also coordinates two water molecules and displays a classical octahedral geometry. In molecule B, the Ca^{2+} ion binds three water molecules, giving rise to pentagonal bipyramidal coordination geometry. In both sites, coordination distances are in the range 2.2–2.5 Å. The bound Ca^{2+} displays a high affinity for the site. Indeed, it has been observed in crystals of PelI grown from protein purified in the presence of the chelating agent EDTA (data not shown). This Ca^{2+} ion is not located in the active site like those identified in PelC but stabilizes a long turn T3 comprising Tyr^{218}.

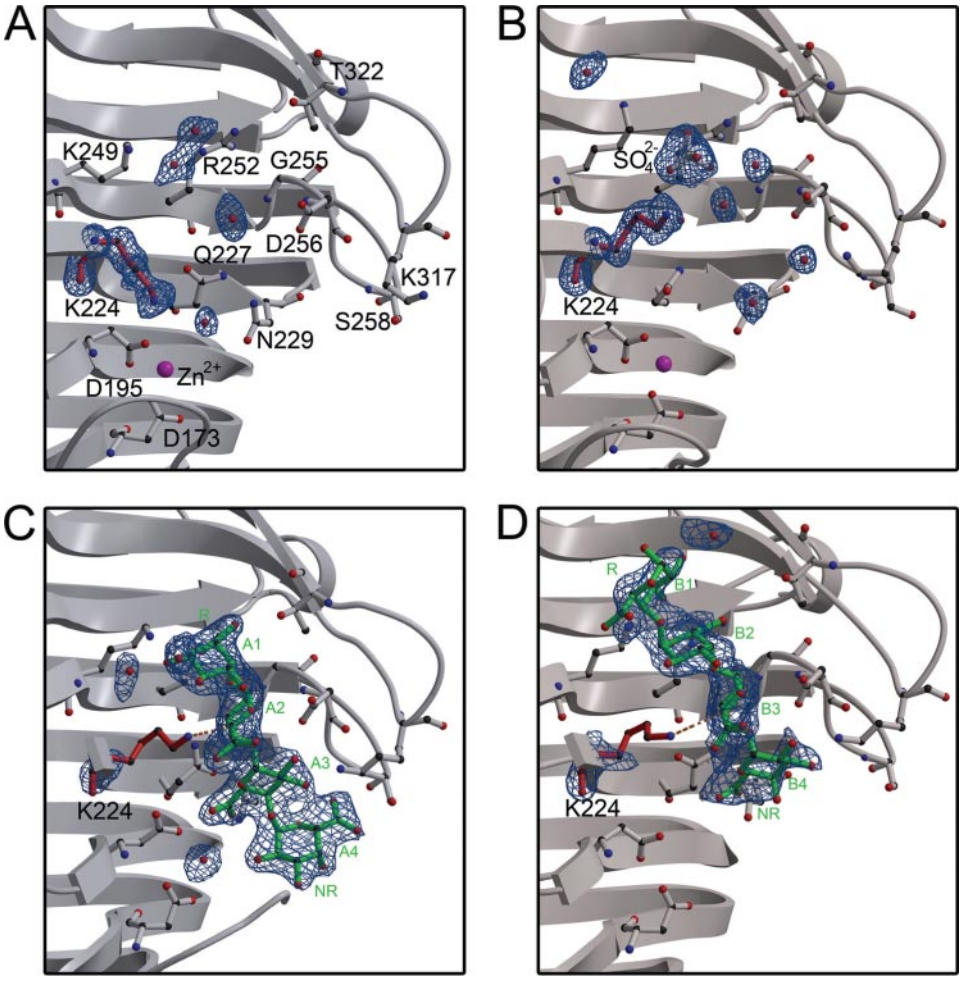

FIGURE 2. **Detailed views of the catalytic sites of PelI with $F_o - F_c$ omit maps.** *A,* substrate-free molecule A. *B,* substrate-free molecule B. *C,* molecule A in complex with a tetrasaccharide. *D,* molecule B in the complex with a tetrasaccharide. Electron density maps have been calculated by omitting the bound sugar and are contoured at 3 σ.

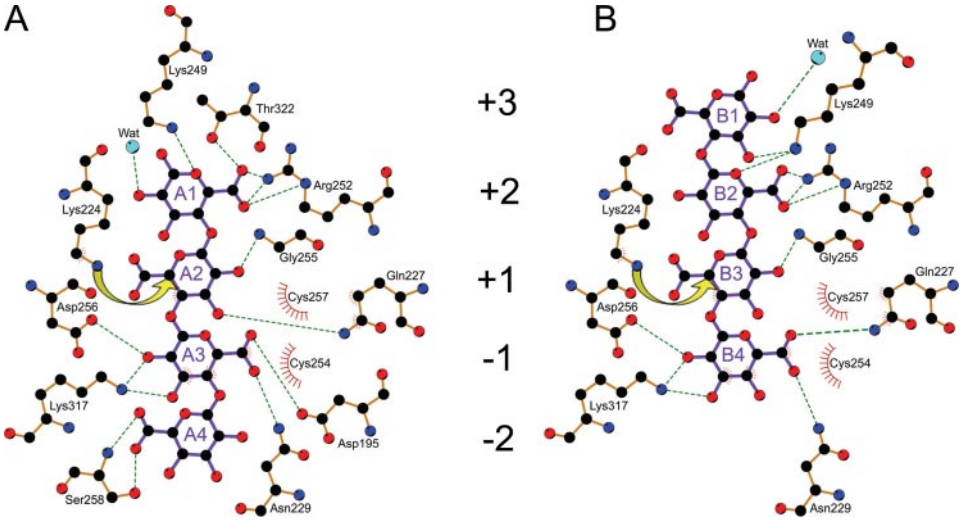

FIGURE 3. **Interactions between the tetrasaccharide and the protein.** *A,* in molecule A. *B,* in molecule B. The moiety Ada1 is at the reducing end (*A1* or *B1*), and the moiety Ada4 is at the non-reducing end (*A4* or *B4*). A *yellow arrow* symbolizes the proton abstraction at the C_5 atom.

This loop is rich in glycine and forms a lid over the bound Ca^{2+} (Fig. 1*A*). A structural Ca^{2+} is found at an equivalent position in Pel-15, crystallized at pH 6.5 (11).

The increase of the pH to 9.5 in Pel-15 involves the binding of a catalytic Ca^{2+} at a neighboring cluster of acidic residues (Asp^{63}, Glu^{83}, and Asp^{84}) in the putative sugar binding site (11). Asp^{63} and Glu^{83} are essential for lyase activity (42), and this acidic cluster is highly conserved among pectate lyases (8, 12, 14). However, in both PelI and $PelI_{cata}$, the two equivalent aspartic residues Asp^{173} and Asp^{195} already coordinate two Zn^{2+} ions provided by the crystallization buffer. These interactions may interfere with the binding of catalytic calcium ions at this site even at alkaline pH. Interestingly, Zn^{2+} ions have a strong inhibitory effect on PelI activity (data not shown). The other Zn^{2+} ions mediate contacts between domains in the crystal. All Zn^{2+} ions display tetrahedral coordination geometry with an average distance of 2.0 Å.

The Conformation of Bound Substrate—The structure of PelI in complex with pectin fragment $GalA_4$ has been determined at a resolution of 2.3 Å after crystal soaking in the absence of calcium. One substrate molecule binds in each molecule A and B to an elongated groove conserved in families PL-1, PL-3, and PL-9. The binding site of PelI stretches from coils 3 to 6, and its base is formed from amino acids of strands PB1. The reducing end of the substrate, termed Ada1, is oriented toward coil 6. The sugar subsites have been identified after superimposition between PelI-$GalA_4$ and inactive PelC-$GalA_5$ (4). One galacturonate unit was not visible in PelC, and the substrate occupies subsites −1 to +3.

Of particular interest in PelI, the substrate binds from subsites −2 to +2 in molecule A, whereas it lies on subsites −1 to +3 in molecule B (Figs. 2 and 3). These two sugar binding modes are consistent with the dual mode of bond cleavage in this substrate. PelI cleaves $GalA_4$ with a frequency of 62% between moieties Ada3 and Ada4 and with a frequency of 38% between moieties Ada2 and Ada3 (43). Thus, the two observed Michaelis complexes perfectly confirm the positions of the two scissile glycosidic bonds in $GalA_4$ acted

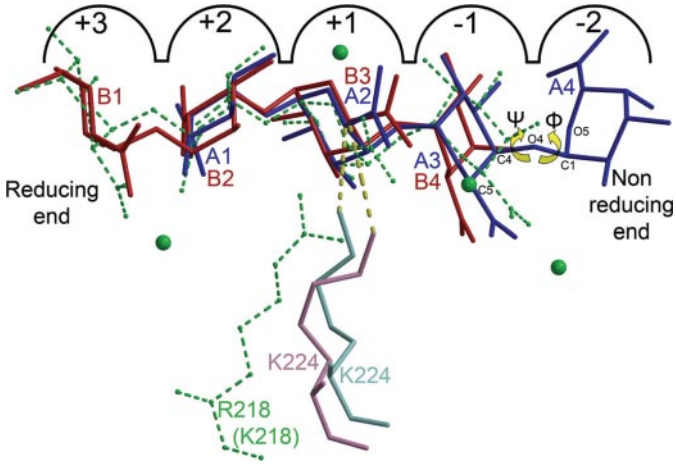

FIGURE 4. **Superimposition between bound sugars in PelI and PelC.** The putative catalytic base Lys^{224} of PelI is colored in shades of *blue* and *red* in monomers A and B, respectively. Bound sugars are colored using the same scheme and are numbered from the reducing end to the non-reducing end (*A1* to *A4* and *B1* to *B4*). Bond angles (τ) and torsional rotations (φ, ψ) about glycosidic bonds are given in supplemental data. Catalytic base Arg^{218}, bound sugar, and catalytic Ca^{2+} ions of PelC are shown in *green*. The essential Arg^{218} has been re-introduced as in the active enzyme.

upon by PelI. In both molecules, the sugar folds so as to form a 2_1 helix (2 units/helical turn) between subsites −1 and +1 and a 3_1 helix between subsites +1 and +2 (Fig. 4). Such distorted helical topology between the essential subsites −1 and +2 has also been reported in PelC and in Pel10Acm complexed with substrate and Ca^{2+} (4, 14). The latter protein exhibits an α-barrel fold, $(\alpha/\alpha)_3$, instead of the classical β-superhelix fold. Therefore, the conserved conformation of the substrate at this central zone −1 to +2 appears to be a requisite for the lyase activity and can be induced even in the absence of Ca^{2+}.

Rearrangements in the Active Site—The structure of PelI-$GalA_4$ indicates that the active site does not overlap with the Fn3D interface on the surface of the catalytic domain. However, in PelI crystals, positive subsites of monomer A and negative subsites of monomer B are partially buried in non-crystallographic interfaces. Monomers A and B shift by ~2 Å with respect to each other during the soaking of PelI crystals with tetrasaccharide. As a consequence, the substrate has gained access to the active site in PelI-$GalA_4$ and loops 144–150 and 215–222 are disordered at these interfaces. These structural constraints at the A/B interfaces are very likely to be responsible for the two sugar binding modes observed in the crystal. They also have an impact on adjacent Asp^{223} and Lys^{224} located at subsite +1 whose side chains are disordered. Beside these structural rearrangements due to the crystal packing, it can be noted that strand PB1′.8, which is poorly conserved in the PL-3 family, has moved by 2 Å in PelI-$GalA_4$ to accommodate the substrate. Hence, Lys^{317} and Thr^{322} come close to the tetrasaccharide to bind it at subsites −1 and +2, respectively (Fig. 3).

Interestingly, the two Zn^{2+} ions coordinated to the acidic cluster in PelI (Asp^{173}, Asp^{195}) disappear in PelI-$GalA_4$ (the soaking experiment was performed in zinc-depleted solutions) and the side chain of Asp^{195} has rotated by 106° around χ_1. It now has a suitable orientation to bind the sugar at subsite −1 (Fig. 2). Finally, a sulfate molecule has been substituted by the substrate at subsite +2 of monomer B (Fig. 2). This sulfate

TABLE 2
Pectate lyase activity detected with the wild-type and mutant proteins
Initial activity rate, in % to wild type, measured in the presence of either 1 mM or 3 mM $CaCl_2$.

	V_o	
	1 mM $CaCl_2$	**3 mM $CaCl_2$**
Wild type	100	100
R252K	6.3	9.1
K249R	38	64
K224R	0.7	0.9

molecule was stabilized by the amine Nζ of Lys^{224} and by the guanidinium of Arg^{252}. The latter residue is the unique arginine of the active site and raises the possibility of it catalyzing the β-elimination of the proton at subsite +1.

The Brønsted Base—In the sugar binding site of PelI, the possible catalytic bases are Lys^{224}, Lys^{249}, and Arg^{252}. It is noteworthy that these three amino acids are invariant in Pel-15 where they display a similar orientation of their side chains.

In PelI-$GalA_4$, the guanidinium group of Arg^{252} firmly binds the carboxylic group of the sugar at subsite +2 (Fig. 3), which prevents any displacement toward subsite +1. The side chain of the neighboring Lys^{249} is also involved in a hydrogen bond with the sugar at subsite +2. This orientation is surprising because Lys^{249} is equivalent in sequence to the catalytic base Arg^{218} of PelC. Thus, a similar extended conformation of its side chain toward subsite +1 (leaving group) was expected. However, Arg^{218} belongs to a turn T3 in PelC and adopts an αL conformation, whereas the isostructural Lys^{249} has a β conformation in PelI. Such divergence in the hydrogen bond network of the two proteins explains the opposite direction taken by the side chains of these two equivalent residues.

The last candidate, Lys^{224}, is the only invariant basic amino acid of the active site in family PL-3 and is well conserved in family PL-1 (Fig. 1*B*). It is close to the flexible segment 215–222, and its side chain is disordered in PelI-$GalA_4$. Nevertheless, its amine function Nζ can point next to the C_5 atom of the sugar at subsite +1 if the orientation of the side chain in substrate-free monomer B is taken as a model (its side chain has another orientation in substrate-free monomer A because it is hydrogen-bonded to Oδ of Asp^{195}). Hence, Lys^{224} seems the best candidate for a catalytic base within PelI. To better address this question, conservative point mutations K224R and K249R, as well as R252K, have been introduced and analyzed (Table 2).

The mutant K224R is completely defective in lyase activity, unlike K249R and R252K, keeping ~40–60% and 6–9% of wild type activity, respectively (Table 2). Interestingly, at a higher Ca^{2+} concentration in the substrate medium, enzymatic activities of K249R and R252K mutants are less affected. Hence, it seems likely that this cation can partially compensate for these mutations either by changing the pK_a of the residues or by altering the substrate conformation. These three mutations maintain the electrostatic character of the binding site, and Lys^{224} appears again as the best candidate catalytic base. A lysine has also been proposed as the catalytic base for Pel9A from family PL-9, although without the support of a liganded structure (12). The putative catalytic bases of PelI and Pel9A are not equivalent in sequence, but their amine functions Nζ are located in similar positions in the active site.

CONCLUSION

Our work demonstrates that modular PelI, despite its 11-amino acid-long loop sequence, is a compact protein with two interacting domains. Notably, the interdomain interface comprises a remarkable pattern of stacked asparagines from the catalytic domain. The hypersensitive response of the plant might be elicited by exposure of this motif (NNGN) following elimination of the Fn3 domain. Hence, the response would be independent of lyase activity as observed in HrpW from *Erwinia amylovora* (44).

Our work also answers the question raised by the structure of Pel-15 (11) by showing that the catalytic base in family PL-3 is not an arginine as in family PL-1, PL-2, and PL-10 but a lysine. The use of a lysine, whose pK_a is 10.5, as a base in enzymes active at pH ~9.0 seems more appropriate than the use of an arginine, whose pK_a is 12.5. Ca^{2+} ions close to the arginine in the Michaelis complex could, however, lower its pK_a to a value that would make the enzyme active (4). The putative catalytic base Lys^{224} of PelI is located one coil below the catalytic base Arg^{218} found in the paradigm PelC from family PL-1 (Fig. 1*B*). The specific activity of PelI on polygalacturonate is lower than that of PelC, and K249R substitution in PelI may have resulted in a PL-1-like efficient enzyme (Lys^{249} in PelI is equivalent to Arg^{218} in PelC), yet this mutant completely lacks activity. Structural comparisons suggest that the key feature is the main-chain conformation of this amino acid, αL in family PL-1 against β in family PL-3.

Our structure of the complex PelI-$GalA_4$ shows that the sugar should bind in pectate lyases with a characteristic distorted helical conformation. It indicates that this topology is not calcium-dependent, although this cation is required for pectate lyase activity. In PelI, the presence of a structural Ca^{2+} ion near the active site may influence the efficiency of the catalytic mechanism. This cation stabilizes the flexible loop 215–222 adjacent to Asp^{223} and the putative catalytic base Lys^{224}. Without this structural Ca^{2+}, the essential Lys^{224} is disordered in PelI-Gal4. Catalytic Ca^{2+} ions certainly bind to the active site of PelI at alkaline pH. In any case, pectate lyases are secreted by bacteria in the plant tissue, where they act on cell wall pectin. Ca^{2+} ions are frequently coordinated to free carboxyl groups of pectin, so catalytic cations can be naturally found complexed with the substrate rather than bound to the enzyme.

The structures of inactive PelC and $GalA_5$ have previously revealed how these catalytic Ca^{2+} ions can mediate interactions between the protein and the sugar at alkaline pH (4). The three Ca^{2+} ions that are unambiguously defined in the electron density maps of PelC (the fourth Ca^{2+} has half occupancy) can be modeled in our structure of PelI in complex with $GalA_4$ with limited structural rearrangements. These ions are of particular interest because, in this configuration, they may connect together deprotonated carboxyl groups of PelI and of the sugar: one Ca^{2+} between Asp^{173}, Asp^{195}, and subsite sugar −1, a second between Asp^{195} and subsite sugar +1, and a third between Asp^{223}, Asp^{256}, and subsite sugar +1. Asp^{223} is invariant in family PL-3 like the adjacent essential Lys^{224}, and a sequence signature -DK- of the active site can be proposed for this family.

A detailed catalytic mechanism has been proposed for Pel9A, with a lysine as a Brønsted base and the support of a More O'Ferrall diagram (12). The interaction of the carboxyl group from the +1 sugar with positive charges can be an important factor for proton abstraction and stabilization of an anionic intermediate. In our high pH model of PelI, the two putative Ca^{2+} ions that are coordinated to the conserved Asp^{195} and Asp^{223} may play this role by connecting the sugar carboxyl. A reasonable assumption is that the transiently protonated base Lys^{224} may then act as the catalytic acid to eliminate the substituent at O_4 and give a C_4–C_5 unsaturated product. Interaction of polar residues with the −1 and +1 sugar oxygen atoms can facilitate the whole reaction (Gln^{227}, Asn^{229}, and Lys^{317} according to Fig. 3).

Finally, the comparison between PelI and PelI-$GalA_4$ sheds new light on the importance of the conserved acidic cluster Asp^{173}, Glu^{194}, and Asp^{195} at the negative subsites. This acidic cluster can favorably complex with Zn^{2+} ions, which results in the obstruction of several Ca^{2+} binding sites and prevents the formation of an active enzyme-substrate complex. Moreover, the side chain of the putative catalytic base Lys^{224} needs to be released from its interaction with Asp^{195} to reach an appropriate orientation at subsite +1 to perform β-elimination. In either PelC or in the complex PelC-$GalA_5$ from family PL-1, the equivalent lysine Lys^{190} is not released from its contact with a similar acidic cluster and the catalytic base is Arg^{218}.

This head-to-head interaction between an acidic and a basic amino acid at the essential −1/+1 subsites evokes the acid-base mechanism observed in family GH28 at acidic pH between the catalytic aspartate and histidine residues (isostructural to Glu^{194}/Asp^{195} and the putative catalytic base Lys^{224} in PelI). Thus, not only do the overall architectures of the modular GH28 and PL-3 resemble one another but the positions of their catalytic residues are also similar. The divergent evolution of carbohydrate-degrading enzymes bearing a β-superhelix fold may have given rise first to the families GH28 and PL-3 and then to family PL-1 with a catalytic base at a distinct position.

Acknowledgment—We thank Harry Kester for tetragalacturonate.

REFERENCES

1. Coutinho, P. M., and Henrissat, B. (1999) in *Recent Advances in Carbohydrate Bioengineering*, (Gilbert, H. J., Davies, G., Henrissat, B., and Svensson, B., eds) pp. 3–12, The Royal Society of Chemistry, Cambridge, UK
2. Shevchik, V. E., Condemine, G., Robert-Baudouy, J., and Hugouvieux-Cotte-Pattat, N. (1999) *J. Bacteriol.* **181,** 3912–3919
3. Abbott, D. W., and Boraston, A. B. (2007) *J. Biol. Chem.* **282,** 35328–35336
4. Scavetta, R. D., Herron, S. R., Hotchkiss, A. T., Kita, N., Keen, N. T., Benen, J. A., Kester, H. C., Visser, J., and Jurnak, F. (1999) *Plant Cell* **11,** 1081–1092
5. Tardy, F., Nasser, W., Robert-Baudouy, J., and Hugouvieux-Cotte-Pattat, N. (1997) *J. Bacteriol.* **179,** 2503–2511
6. Shevchik, V. E., Boccara, M., Vedel, R., and Hugouvieux-Cotte-Pattat, N. (1998) *Mol. Microbiol.* **29,** 1459–1469
7. Yoder, M. D., Lietzke, S. E., and Jurnak, F. (1993) *Structure* **1,** 241–251
8. Nakaniwa, T., Tada, T., Ishii, K., Takao, M., Sakai, T., and Nishimura, K. (2003) *Acta Crystallogr. Sect. D Biol. Crystallogr.* **59,** 341–342
9. Thomas, L. M., Doan, C. N., Oliver, R. L., and Yoder, M. D. (2002) *Acta Cryst. Sect. D Biol. Crystallogr.* **58,** 1008–1015
10. Pickersgill, R., Jenkins, J., Harris, G., Nasser, W., and Robert-Baudouy, J.

(1994) *Nat. Struct. Biol.* **1,** 717–723
11. Akita, M., Suzuki, A., Kobayashi, T., Ito, S., and Yamane, T. (2001) *Acta Cryst. Sect. D Biol. Crystallogr.* **57,** 1786–1792
12. Jenkins, J., Shevchik, V. E., Hugouvieux-Cotte-Pattat, N., and Pickersgill, R. W. (2004) *J. Biol. Chem.* **279,** 9139–9145
13. Novoa De Armas, H., Verboven, C., De Ranter, C., Desair, J., Vande Broek, A., Vanderleyden, J., and Rabijns, A. (2004) *Acta Cryst. Sect. D Biol. Crystallogr.* **60,** 999–1007
14. Charnock, S. J., Brown, I. E., Turkenburg, J. P., Black, G. W., and Davies, G. J. (2002) *Proc. Natl. Acad. Sci. U. S. A.,* **99,** 12067–12072
15. Pickersgill, R., Smith, D., Worboys, K., and Jenkins, J. (1998) *J. Biol. Chem.* **273,** 24660–24664
16. Abbott, D. W., and Boraston, A. B. (2007) *J. Mol. Biol.* **368,** 1215–1222
17. Michel, G., Pojasek, K., Li, Y., Sulea, T., Linhardt, R. J., Raman, R., Prabhakar, V., Sasisekharan, R., and Cygler, M. (2004) *J. Biol. Chem.* **279,** 32882–32896
18. Van Petegem, F., Contreras, H., Contreras, R., and Van Beeumen, J. (2001) *J. Mol. Biol.* **312,** 157–165
19. Liu, Y., Chatterjee, A., and Chatterjee, A. K. (1994) *Appl. Environ. Microbiol.* **60,** 2545–2552
20. Login, F. H., and Shevchik, V. E. (2006) *J. Biol. Chem.* **281,** 33152–33162
21. Buttner, D., and Bonas, U. (2003) *Curr. Opin. Plant. Biol.* **6,** 312–319
22. Castang, S., Shevchik, V. E., Hugouvieux-Cotte-Pattat, N., Legrand, P., Haser, R., and Gouet, P. (2004) *Acta Cryst. Sect. D Biol. Crystallogr.* **60,** 190–192
23. Brünger, A. T., Adams, P. D., Clore, G. M., DeLano, W. L., Gros, P., Grosse-Kunstleve, R. W., Jiang, J. S., Kuszewski, J., Nilges, M., Pannu, N. S., Read, R. J., Rice, L. M., Simonson, T., and Warren, G. L. (1998) *Acta Cryst. Sect. D Biol. Crystallogr.* **54,** 905–921
24. Roussel, A., and Cambillau, C. (1992) TURBO-FRODO, Biographics, AFMB, Marseille, France
25. Laskowski, R. A., MacArthur, M. W., Moss, D. S., and Thornton, J. M. (1993) *J. Appl. Crystallogr.* **26,** 283–291
26. Navaza, J. (2001) *Acta Cryst. Sect. D Biol. Crystallogr.* **57,** 1367–1372
27. Frishman, D., and Argos, P. (1995) *Proteins* **23,** 566–579
28. Holm, L., and Park, J. (2000) *Bioinformatics* **16,** 566–567
29. Gouet, P., Robert, X., and Courcelle, E. (2003) *Nucleic Acids Res.* **31,** 3320–3323
30. Wallace, A. C., Laskowski, R. A., and Thornton, J. M. (1995) *Protein Eng.* **8,** 127–134
31. Kraulis, P. J. (1991) *J. Appl. Crystallogr.* **24,** 946–950
32. Esnouf, R. (1999) *Acta Cryst. Sect. D Biol. Crystallogr.* **55,** 938–940
33. Yang, Z. R., Thomson, R., McNeil, P., and Esnouf, R. M. (2005) *Bioinformatics* **21,** 3369–3376
34. Jee, J. G., Ikegami, T., Hashimoto, M., Kawabata, T., Ikeguchi, M., Watanabe, T., and Shirakawa, M. (2002) *J. Biol. Chem.* **277,** 1388–1397
35. Huber, A. H., Wang, Y. M., Bieber, A. J., and Bjorkman, P. J. (1994) *Neuron* **12,** 717–731
36. Bork, P., and Doolittle, R. F. (1993) *Protein Sci.* **2,** 1185–1187
37. Sharma, A., Askari, J. A., Humphries, M. J., Jones, E. Y., and Stuart, D. I. (1999) *EMBO J.* **18,** 1468–1479
38. Leahy, D. J., Hendrickson, W. A., Aukhil, I., and Erickson, H. P. (1992) *Science* **258,** 987–991
39. Ingham, K. C., Brew, S. A., Migliorini, M. M., and Busby, T. F. (1993) *Biochemistry* **32,** 12548–12553
40. Kataeva, I. A., Seidel, R. D., III, Shah, A., West, L. T., Li, X. L., and Ljungdahl, L. G. (2002) *Appl. Environ. Microbiol.* **68,** 4292–4300
41. Boraston, A. B., Bolam, D. N., Gilbert, H. J., and Davies, G. J. (2004) *Biochem. J.* **382,** 769–781
42. Hatada, Y., Kobayashi, T., and Ito, S. (2001) *Extremophiles* **5,** 127–133
43. Roy, C., Kester, H., Visser, J., Shevchik, V., Hugouvieux-Cotte-Pattat, N., Robert-Baudouy, J., and Benen, J. (1999) *J. Bacteriol.* **181,** 3705–3709
44. Kim, J. F., and Beer, S. V. (1998) *J. Bacteriol.* **180,** 5203–5210